Models for the a subunits of the *Thermus thermophilus* V/A-ATPase and *Saccharomyces cerevisiae* V-ATPase enzymes by cryo-EM and evolutionary covariance

Daniel G. Schep[a,b], Jianhua Zhao[a,b], and John L. Rubinstein[a,b,c,1]

[a]The Hospital for Sick Children Research Institute, Toronto, ON, Canada M5G0A4; [b]Department of Medical Biophysics, The University of Toronto, Toronto, ON, Canada M5G1L7; and [c]Department of Biochemistry, The University of Toronto, Toronto, ON, Canada M5S1A8

Edited by Eva Nogales, University of California, Berkeley, CA, and approved February 3, 2016 (received for review November 9, 2015)

Rotary ATPases couple ATP synthesis or hydrolysis to proton translocation across a membrane. However, understanding proton translocation has been hampered by a lack of structural information for the membrane-embedded a subunit. The V/A-ATPase from the eubacterium *Thermus thermophilus* is similar in structure to the eukaryotic V-ATPase but has a simpler subunit composition and functions in vivo to synthesize ATP rather than pump protons. We determined the *T. thermophilus* V/A-ATPase structure by cryo-EM at 6.4 Å resolution. Evolutionary covariance analysis allowed tracing of the a subunit sequence within the map, providing a complete model of the rotary ATPase. Comparing the membrane-embedded regions of the *T. thermophilus* V/A-ATPase and eukaryotic V-ATPase from *Saccharomyces cerevisiae* allowed identification of the α-helices that belong to the a subunit and revealed the existence of previously unknown subunits in the eukaryotic enzyme. Subsequent evolutionary covariance analysis enabled construction of a model of the a subunit in the *S. cerevisae* V-ATPase that explains numerous biochemical studies of that enzyme. Comparing the two a subunit structures determined here with a structure of the distantly related a subunit from the bovine F-type ATP synthase revealed a conserved pattern of residues, suggesting a common mechanism for proton transport in all rotary ATPases.

cryo-EM | evolutionary covariance | V-ATPase | V/A-ATPase | structure

Vacuolar H^+-ATPases (V-ATPases) are large membrane protein complexes responsible for the acidification of intracellular compartments in eukaryotes. These complexes are essential for processes including receptor-mediated endocytosis, coupled transport, and lysosomal degradation (1). V-ATPases localize to the plasma membrane of some specialized cells where they participate in bone resorption by osteoclasts (2) and urine acidification by the α-intercalated cells of the kidney (3). Malfunction or misregulation of these enzymes results in numerous disorders, including osteopetrosis (4) and renal tubular acidosis (5, 6). Expression of V-ATPases on the surfaces of some tumor cells results in increased tumor invasion and metastasis (7). The V/A-ATPase from the thermophilic eubacterium *Thermus thermophilus* is homologous to the eukaryotic V-ATPase and has a similar overall structure, but is smaller and simpler and functions in vivo as an ATP synthase. V- and V/A-ATPases have similar subunit folds and arrangements of subunits (8–11). The simplified architecture and superior stability of the *T. thermophilus* V/A-ATPase make it an ideal model to study the structure and function of V-ATPases. Both enzymes are composed of a soluble V_1 catalytic region and a membrane-embedded V_O region. The V/A-ATPase subunits I, L, and C in *T. thermophilus* are homologous to the a, c, and d subunits in eukaryotic V-ATPases, respectively, and, for clarity, the eukaryotic subunit names are used here. With this convention, the *T. thermophilus* V/A-ATPase contains subunits $A_3B_3DE_2FG_2ac_{12}d$ whereas the eukaryotic V-ATPase from *Saccharomyces cerevisiae* contains subunits $A_3B_3CDE_3FG_3Hac_xc'_yc''_zde$, with x, y, and z denoting unknown stoichiometries (Fig. S1). Uppercase letter names indicate components of the V_1 region, and lowercase letters denote components of the V_O region. The V_1 and V_O regions are connected by a central rotor subcomplex (subunits D, F, d, and the c-ring) and heterodimeric peripheral stator subcomplexes (subunits E and G). The V_O region couples the transport of protons across the membrane to the rotation of the central rotor whereas the V_1 region couples the rotation of the central rotor to ATP synthesis or hydrolysis. In the *T. thermophilus* V/A-ATPase, the V_O region is embedded in the plasma membrane and the V_1 region is in the cytoplasm, with protons flowing from the periplasm to the cytoplasm during ATP synthesis.

High-resolution crystal structures are available for nearly all subunits of the *T. thermophilus* V/A-ATPase (10, 12, 13) or for close homologs from other organisms (14, 15). However, no crystal structure exists for the membrane-integral C-terminal domain of the a subunit. The a subunit contacts the membrane-embedded c_{12}-ring, and together the a and c subunits transport protons through the complex and cause rotation of the central rotor. A popular model for proton transport involves two offset half-channels present at the a/c subunit interface (9, 16, 17). In this model, a periplasmic half-channel shuttles protons from the periplasm halfway across the membrane to the conserved E63 residue of one of the c subunits. Protonation by the periplasmic half-channel neutralizes the charge of the glutamate residue, allowing the c_{12}-ring to rotate away from the a subunit so that the glutamate residue is placed into the hydrophobic environment of

Significance

In cells, chemical energy is interconverted with electrochemical ion gradients across membranes for numerous processes. Three of the most significant enzymes that carry out this conversion are known as rotary ATPases because ion translocation is coupled to the synthesis or hydrolysis of ATP by rotation of part of the enzyme. These protein assemblies are the closely related eukaryotic V-ATPases and bacterial or archaeal V/A-ATPases, and the more distantly related F-type ATP synthases. Understanding of rotary ATPases has been limited by not knowing the structure of the subunit that couples ion translocation to rotation. Here, we determine the structure of this subunit for two of the three types of rotary ATPases, identifying a conserved architecture and mechanism in all three enzymes.

Author contributions: D.G.S. and J.L.R. designed research; D.G.S. and J.Z. performed research; D.G.S. and J.L.R. analyzed data; D.G.S. and J.L.R. wrote the paper; and J.L.R. designed the project and supervised research.

The authors declare no conflict of interest.

This article is a PNAS Direct Submission.

Data deposition: All cryo-EM maps described in this manuscript have been deposited in the Electron Microscopy Data Bank (EMDB) (accession nos. EMD-8016, EMD-8017, and EMD-8070). Atomic models have been deposited in the Protein Data Bank, www.pdb.org (PDB ID codes 5GAR, 5GAS, and 5I1M).

[1]To whom correspondence should be addressed. Email: john.rubinstein@utoronto.ca.

This article contains supporting information online at www.pnas.org/lookup/suppl/doi:10.1073/pnas.1521990113/-/DCSupplemental.

the lipid bilayer. Rotation of the ring delivers a protonated glutamate residue from within the lipid bilayer to a cytoplasmic half-channel where the residue releases its proton into the cytoplasm.

Previous maps of the V/A-ATPase from cryo-EM have shown that the contact between the a subunit and c_{12}-ring is small (9, 18). Cryo-EM of the *S. cerevisiae* V-ATPase has also shown that where the a subunit contacts the c-ring it is composed of two long and highly tilted α-helices (8). Cryo-EM and low-resolution X-ray crystallography have resolved these long and tilted α-helices in the F-type ATP synthase from the algae *Polytomella* sp. (19), the mammal *Bos taurus* (20), and the bacterium *Paracoccus denitrificans* (21). Identification of covarying pairs of residues in the sequences of homologous proteins, also known as evolutionary couplings, can identify pairs of residues that are likely to interact physically (22–25). A model was proposed for the a subunit from the mammalian ATP synthase using data from evolutionary covariance in conjunction with the cryo-EM density map (20). This atomic model of the *B. taurus* ATP synthase a subunit was shown to be accurate by an X-ray crystallography model of the a subunit from *P. denitrificans* that was published almost simultaneously with the *B. taurus* model, but which was not available when the modeling was done (21).

In the work described here, we calculated a cryo-EM map of the intact *T. thermophilus* V/A-ATPase at 6.4 Å resolution and built a model of the membrane-embedded a subunit into the map with constraints from evolutionary covariance (22). Using information from the V/A-ATPase a subunit map and model, we also generated a model of the homologous a subunit from the *S. cerevisiae* V-ATPase, which shows that there are unidentified subunits in the V_O region of the eukaryotic V-ATPase. Numerous biochemical studies of the *S. cerevisiae* V-ATPase support these a subunit models. Comparison of the a subunit models from the V/A-ATPase, V-ATPase, and F-type ATP synthase reveals similarities in positioning of several conserved residues despite large differences in the sequence and overall fold of the F-type enzyme. These models of the membrane-embedded a subunits in V/A-, V-, and F-type enzymes suggest a path for protons through the membrane-embedded regions and several key residues involved in the process.

Results

Structure of the V/A-ATPase. Samples of *T. thermophilus* V/A-ATPase were purified and imaged by cryo-EM as described previously (18) with slight modifications (Methods). A map of the enzyme at 6.4 Å resolution was calculated from 197,178 particle images (Fig. 1*A* and Fig. S2). Estimation of local resolution in the map indicated that the V_1 region is better resolved than the V_O region (Fig. S2*D*), as observed previously for the eukaryotic V-ATPase (8). Analysis of image tilt pairs (Fig. S3) showed an image alignment accuracy similar to the accuracy seen with *T. thermophilus* V/A-ATPase data collected on photographic film (26, 27). Available crystal structures (10, 12, 13) and homology models (14, 15) were fit into the V/A-ATPase map using molecular dynamics flexible fitting (MDFF), showing that the enzyme complex adopts the same rotational state as seen in previous maps (9, 18) (Fig. 1*A*). This rotational state has the central rotor positioned so that the F subunit is almost equidistant to the two peripheral stalks.

Cryo-EM Maps Show the Architecture of the a Subunit. The cryo-EM map of the V/A-ATPase shows clearly the arrangement of all eight membrane-embedded α-helices in the a subunit as elongated densities (Fig. 1 *A*, green density, and *B*). This a subunit map segment can be compared with homologous subunits in the V-ATPase and F-type ATP synthase, which display similar features despite limited sequence conservation. To increase the local resolution of the V_O region in the *S. cerevisiae* V-ATPase map (8), six different maps of this enzyme in different rotational states and with different cofactors bound (Methods) were aligned by their a subunits and averaged (Fig. 1*C*). The a subunit

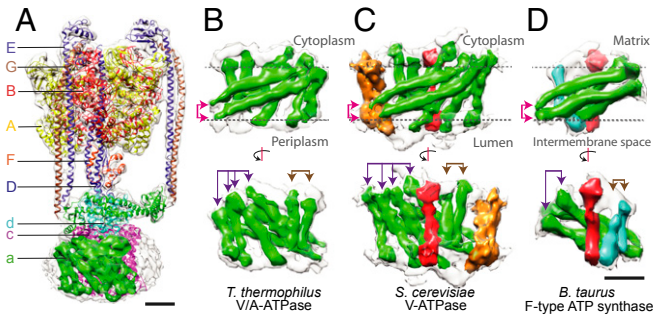

Fig. 1. Common architecture of a subunits from different rotary ATPases. (*A*) The *T. thermophilus* V/A-ATPase map allowed the fitting of crystal structures and homology models, as well as the identification of transmembrane α-helices in the a subunit (green density). Similar arrangements of α-helices in the a subunit are observed in the *T. thermophilus* V/A-ATPase (*B*), the *S. cerevisiae* V-ATPase (*C*), and the *B. taurus* F-type ATP synthase (*D*), indicated by the magenta, violet, and brown arrows. The V-ATPase and F-type ATP synthase share a common feature not found in the V/A-ATPase (*C* and *D*, red density). Additional density is observed in the *S. cerevisiae* V-ATPase that is not present in the other rotary ATPases (*C*, orange density). Cyan densities in *D* are from the b subunit in the F-type ATP synthase. (Scale bars: 25 Å.)

in all three enzymes contains two long, tilted α-helices forming a hairpin that contacts the c-ring (Fig. 1 *B–D*, *Upper*, magenta arrows). Both the V/A- and V-ATPase a subunits each have four slightly tilted and nearly parallel α-helices located adjacent to this hairpin, in the same location and at a similar angle to a second hairpin of α-helices in the F-type ATP synthase a subunit (Fig. 1 *B–D*, *Lower*, violet arrows). Furthermore, all three rotary ATPases also contain two parallel α-helices, perpendicular to the membrane, near the periplasmic end of the hairpin that contacts the c-ring (Fig. 1 *B–D*, *Lower*, brown arrows). In the F-type ATP synthase, these two α-helices are not from the a subunit, but are part of the b subunit. Every α-helix in the V/A-ATPase a subunit has a corresponding α-helix in the V-ATPase (Fig. 1 *B* and *C*, green density). However, the *S. cerevisiae* V_O region also contains density not found in the *T. thermophilus* V/A-ATPase. A density in the V-ATPase, likely consisting of one or two α-helices perpendicular to the membrane and distal to the c_{10}-ring, is located in the same position as the N-terminal α-helix of the F-type ATP synthase a subunit (Fig. 1 *C* and *D*, red density). An additional membrane-spanning density is also present abutting the a subunit in the yeast V-ATPase that has no equivalent in the other maps (Fig. 1*C*, orange density). In addition to the c_{10}-ring and subunit a, the only other proposed subunit in the V_O region of the *S. cerevisiae* V-ATPase is subunit e, which is not necessary for proton translocation in vitro (28). The discovery of membrane-protein subunits in the cryo-EM map of the V-ATPase is not surprising. The two additional densities seem to be transmembrane proteins without obvious soluble regions. Hydrophobic proteins often do not stain well in SDS/PAGE and lack the Lys and Arg residues needed for identification of proteins with trypsin digestion and mass spectrometry, and hydrophobic peptide fragments from proteins may bind irreversibly to the chromatography columns used in the preparation of mass spectrometry samples. For these reasons, novel membrane-protein subunits continue to be detected for large hydrophobic protein complexes, such as the mitochondrial ATP synthase and complex I, despite many decades of study (29, 30). V-ATPase subunit mutations often cause the slow-growing *VMA* phenotype in yeast, allowing for identification of V-ATPase subunits from the phenotype of cells where they are mutated. However, mutation of subunits that are not essential for the proton-pumping activity of the enzyme would not be expected to cause this phenotype. It is unlikely that the additional densities are derived from a portion of the a subunit that re-enters the lipid

bilayer because no suitably positioned loop is both long and hydrophobic enough to form an additional transmembrane α-helical hairpin. Also, extensive biochemical labeling experiments have determined that this subunit consists of eight membrane-embedded α-helices (31). It is possible that one of these densities corresponds to the e subunit that was not detected in the study that determined that it is not necessary for proton pumping in vitro (28). However, it remains undetermined what proteins give rise to the additional densities in the V_O region of the eukaryotic V-ATPase.

Model of the *T. thermophilus* a Subunit. We constructed a model for the C-terminal domain of the *T. thermophilus* V/A-ATPase a subunit using the 6.4-Å cryo-EM map and constraints from evolutionary covariance analysis. Analysis of evolutionary covariance in the N-terminal domain of the *Meiothermus ruber* V/A-ATPase a subunit (Fig. S4*A*), where a crystal structure is known (15), demonstrates a sufficient number of available sequences to obtain structural insight for the V/A-ATPase a subunit. Covarying residues were identified for the membrane-integral domain of the *T. thermophilus* V/A-ATPase subunit a and the 100 highest-scoring evolutionary couplings were included in the structural analysis as constraints (Fig. S4*B*). A model was created for the domain that minimized the distance between predicted coevolving pairs of residues in the membrane-embedded α-helices. Loops connecting these α-helices were modeled with *Rosetta* (32, 33). The resulting model (Fig. 2*A*, and Movie S1) has its C terminus on the cytoplasmic side of the membrane, near the link between the N- and C-terminal domains of the protein. The N-terminal α-helix (Fig. 2*A*, α-helix 1, blue) extends from the cytoplasmic surface partway into the expected position of the lipid bilayer, slightly tilted with respect to the membrane, before returning to the cytoplasmic surface in a second α-helix (Fig. 2*A*, α-helix 2) perpendicular to the membrane. This second α-helix is closely associated with, and antiparallel to, the third transmembrane α-helix (Fig. 2*A*, α-helix 3). The next three α-helices (Fig. 2*A*, α-helices 4–6) are slightly tilted with respect to the expected plane of the lipid bilayer, and the final two α-helices (Fig. 2*A*, α-helices 7 and 8) form the tilted α-helical hairpin in contact with the c_{12}-ring. α-helices 1 through 6 form an N-terminal layer distal to the c_{12}-ring whereas α-helices 7 and 8 form the C-terminal hairpin that contacts the c_{12}-ring. This model places the conserved and essential R563 (34) (Fig. 2*A*, brown sphere) near the center of the C-terminal hairpin in the same approximate position as was seen for the essential arginine in the *B. taurus* F-type ATP synthase (20).

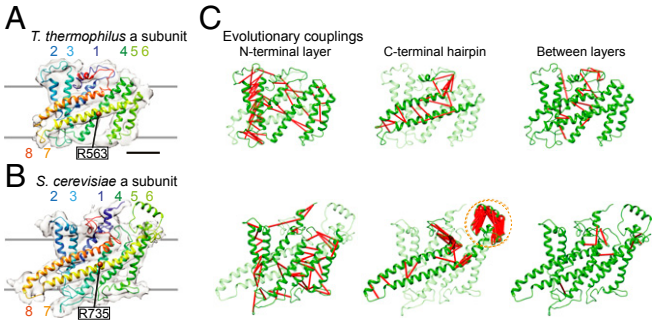

Fig. 2. Models of the proton-translocating a subunit. Subunit a models from *T. thermophilus* V/A-ATPase (*A*) and *S. cerevisiae* V-ATPase (*B*) show a similar fold and placement of the conserved and essential arginine (brown spheres). (*C*) The models minimize the distance between covarying residues (red lines) while optimizing the polypeptide fit in the cryo-EM density map. For clarity, covarying residue pair connections are shown as red sticks separately in the N-terminal layer composed of helices 1 through 6, the C-terminal hairpin of helices 7 and 8, and connections between these layers. The 10% of covarying amino acid pairs with the longest inter-Cα distance were omitted in the figure. The average distance of the remaining constraints was 11.2 Å for the *T. thermophilus* V/A-ATPase a subunit and 12.8 Å for the *S. cerevisiae* V-ATPase a subunit. A large number of covarying residues are found in the cytoplasmic loop connecting α-helices 6 and 7 of the V-ATPase a subunit (dashed orange circle). (Scale bar: 25 Å.)

Model of the *S. cerevisiae* a Subunit. Like the *T. thermophilus* V/A-ATPase a subunit, the V-ATPase a subunit has been predicted to contain eight membrane-embedded α-helices (31). Aligning the a subunit sequences from the *T. thermophilus* V/A-ATPase and *S. cerevisiae* V-ATPase reveals 16% identity and 32% similarity (Fig. S5). Given that the *S. cerevisiae* and *T. thermophilus* a subunits are expected to have the same fold with the same number of transmembrane α-helices, a model for the *S. cerevisiae* a subunit was created (Fig. 2*B*) incorporating evolutionary covariance constraints and using only the α-helical densities that were present in both the V-ATPase and V/A-ATPase maps (Fig. 2*C*, *Lower*, red lines, Fig. S4*C*, and Movie S2). Aligning both a subunit sequences showed that the placement of transmembrane α-helices largely overlaps, mostly in areas with high sequence similarity (Fig. S5). Despite both proteins containing the same number of transmembrane α-helices, the V-ATPase a subunit C-terminal domain sequence is 128 residues longer then the V/A-ATPase a subunit. This difference in length is partly due to differing α-helix lengths, but mostly because of the presence of large, membrane-extrinsic loops found only in the eukaryotic enzyme. The presence of a large cytoplasmic loop in the V-ATPase a subunit consisting of residues 655–707, which includes long stretches of charged residues, is a significant difference between the two enzymes (Fig. 2*C*, dashed orange circle). Furthermore, of the 200 covarying pairs of residues initially used to build the V-ATPase a subunit model, 94 are within this loop. This strong evolutionary covariance suggests an important role for the loop in V-ATPase function (24). The existence of covariance in this loop region would not be expected to affect the detection of covariance in the rest of the subunit. Considering its placement near the cytoplasmic half-channel, this highly charged loop may modulate the a subunit's affinity for protons entering the V_O region from the cytoplasm, a role that is not required in F-type ATP synthase or V/A-ATPase enzymes. V-ATPase activity is modulated by reversible dissociation of the V_1 and V_O regions (35, 36), and different isoforms of the eukaryotic V-ATPase a subunit target the enzyme to specific cellular locations (37). The loop differs significantly between the two *S. cerevisiae* isoforms of the a subunit, Vph1p and Stv1p, which have an overall sequence identity of 50%, but only 15% sequence identity within this loop. Thus, this region of the a subunit may be responsible for modifying the activity or regulation of the different subunit isoforms to fulfill the varying roles of V-ATPase in different cellular compartments. Although there are eight constraints between the "layers" of the *S. cerevisiae* V-ATPase a subunit shown in Fig. 2*B*, only the proposed fold for the subunit is able to simultaneously satisfy the majority of these constraints between layers and the other constraints considered.

Rotational States of the *T. thermophilus* V/A-ATPase. Other than the linker between the soluble N-terminal domain and membrane-embedded C-terminal domain of the a subunit, this a subunit model gives, to our knowledge, the first complete atomic model of the *T. thermophilus* V/A-ATPase (Fig. 3*A*). Difference maps between the atomic model and the experimental map show that the only density missing from the model is the detergent micelle, the a subunit linker region, and density that corresponds to the N and C termini of the A and B subunits (Fig. S6, green density) that are missing in the V_1 crystal structure (12). Three-dimensional classification of the data used to obtain the V/A-ATPase map also identified a small, and likely inhomogeneous, subpopulation of images that yielded a map in a second rotational state (Fig. 3*F*). The second conformation differs from the first by an ~120° rotation of the central rotor, clockwise when viewed from the V_1 region toward the V_O region (Fig. 3 *B* and *D*, green circles), as well as by having a different arrangement of tight,

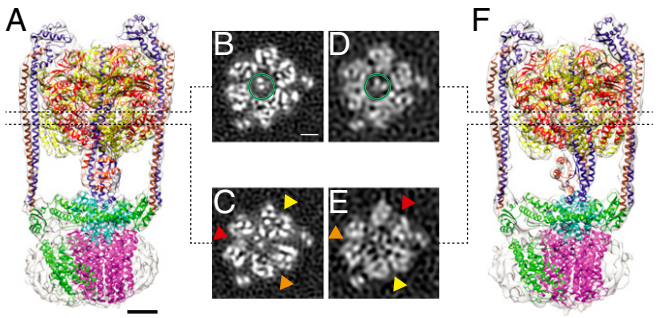

Fig. 3. Two rotational states of *T. thermophilus* V/A-ATPase. Crystal structures, homology models, and the a subunit model were fit into the maps of the V/A-ATPase in two different conformations (*A* and *F*). Sections through the maps reveal that the main structural difference between the conformations is the position of the central rotor (*B* and *D*, green circle). Each catalytic AB pair in each map is in an open (red), loose (orange), or tight (yellow) state (*C* and *E*, arrows), and the arrangement of conformations is different in the two maps. (Scale bars: 25 Å.)

loose, and open conformations of the AB pairs (Fig. 3 *C* and *E*, arrows). Other than these differences, comparison of the two states reveals only minor conformational changes in individual subunits, suggesting little flexibility in the enzyme as a whole (Movie S3). The *T. thermophilus* V/A-ATPase thus seems to be relatively rigid compared with the *S. cerevisiae* V-ATPase (8) and *B. taurus* F-type ATP synthase (20) where more highly populated rotational states were identified. The lack of observed flexibility may be a result of the symmetry-matched V_1 and V_O regions in the *T. thermophilus* V/A-ATPase, where the catalytic and membrane-embedded regions have 3 and 12 rotational positions, respectively. In comparison, the *S. cerevisiae* V-ATPase has a 3:10 symmetry mismatch, and the *B. taurus* ATP synthase has a 3:8 symmetry mismatch. The uneven distribution of particle images between the two classes suggests that the highly populated class represents an energetically favorable ground state of the enzyme.

Biochemical Studies Support the Model of the *S. cerevisiae* a Subunit. Numerous studies, many by Forgac and coworkers, have investigated the topology, function, and subunit arrangement of the *S. cerevisiae* V-ATPase V_O region (31, 34, 38–44). The model of the a subunit presented here is in excellent agreement with these studies. First, the model agrees well with experiments that probed topology and accessibility of the a subunit by labeling residues mutated to cysteine to define them as luminal, membrane-embedded, cytoplasmic, or at the cytoplasmic border (31, 38, 39) (Fig. 4*A*). All of the locations of residues identified by these studies are consistent with their locations in the model presented here. Some residues identified as luminal or on the cytoplasmic border seem to be within the lipid bilayer in Fig. 4*A*. It is possible that the labeling of residues past the membrane border is the result of the aqueous channels that allow proton transport by the subunit. By identifying mutations that reduce V-ATPase activity, previous work has also defined the a subunit residues likely involved in proton translocation (31, 34, 40, 41). Our model of the a subunit places the identified residues either between or near the critical E137 residue of the two adjacent c subunits (Fig. 4*B*). Most of the amino acids identified are in the ring-contacting α-helices 7 and 8, except for two highly conserved membrane-embedded aspartate residues: D425 on the short linker connecting α-helices 1 and 2, and D481 on α-helix 3. In addition, cysteine-mediated cross-linking has helped define the location of specific a subunit residues in relation to the c′ subunit (42). These cross-linking results also agree well with the proposed a subunit model (Fig. 4*C*), with distances between cross-linked residues of 6.4 Å to 17 Å. Finally, studies of the a and c subunits identified residues that, when mutated, can lead to partial resistance to bafilomycin, an inhibitor of V-ATPases. Single and double mutants were made in the c subunit of *Neurospora crassa*, a mold whose c subunit sequence is 79% identical to that of the *S. cerevisiae* c subunit (43). Ten residues were proposed to participate in bafilomycin binding, all of which are conserved in *S. cerevisiae*. In addition, three a subunit residues were identified in *S. cerevisiae* where mutation conferred bafilomycin resistance (44). Visualizing these residues together suggests a binding site for bafilomycin between two c subunits accessible from the cytoplasm through the a subunit (Fig. 4*D*).

Discussion

The similarities between the a subunit structures presented here and previously (20) allow us to identify conserved features in these subunits from the three types of rotary ATPases, suggesting a model for proton translocation. All rotary ATPases include an essential membrane-embedded arginine residue in the a subunit: R563 in the *T. thermophilus* V/A-ATPase, R735 in the *S. cerevisiae* V-ATPase, and R159 in the *B. taurus* F-type ATP synthase (34, 45). The three models of different a subunits show that a similar arrangement of residues surround the essential arginine near the c subunit α-helices in all three proteins (Fig. 5 *A*–*C*). Mutation of these residues in the yeast V-ATPase has been shown to decrease enzyme activity (31, 40). One c subunit α-helix is close to a conserved pair of residues in the a subunits where one residue has an acidic side chain and the other bears a hydroxyl group: E550/T553 in V/A-ATPase, E721/S728 in V-ATPase, and E145/S148 in F-type ATP synthase (Fig. 5 *A*–*C*, orange). Another c subunit is close to the basic residue H616 in V/A-ATPase, H743 in V-ATPase, and H168 in F-type ATP synthase (Fig. 5 *A*–*C*, blue). These histidines are located on the penultimate ring-contacting α-helix in the V-ATPase and bovine F-type ATP synthase, but on the C-terminal α-helix in the *T. thermophilus* V/A-ATPase. In the bovine F-type ATP synthase and yeast V-ATPase, the histidine is in close proximity to a glutamate on the C-terminal α-helix that is implicated in proton transport (E789 and E203, respectively). However, this additional glutamate is not present in the V/A-ATPase a subunit, possibly because membrane proteins from thermophilic organisms generally have fewer membrane-embedded charged residues (46). The *Escherichia coli* F-type

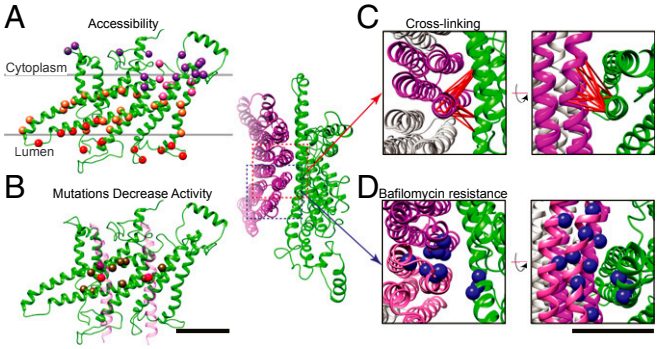

Fig. 4. Comparison of the V-ATPase a subunit model with existing biochemical data. (*A*) Experiments determining accessibility of amino acids defined residues as residing in the cytoplasm (purple spheres), at the cytoplasmic border (pink spheres), in the lumen (red spheres), or within the membrane (orange spheres) (31, 38, 39). Approximate membrane borders are shown in gray. (*B*) Mutagenesis of residues (brown spheres) severely reduces activity in the V-ATPase: D425, D481, E721, S728, R735, E789, S792, H796, R799, and H801 (31, 34, 40, 41). Two adjacent c subunits are shown (transparent magenta ribbon) bearing the essential E137 (red spheres). (*C*) Cysteine-mediated cross-linking (red lines) of one c′ subunit (magenta) to subunit a (green) (42). (*D*) Residues that, when mutated (blue spheres) in the c subunit (T32, T39, L50, I54, V57, G61, L131, F135, L139, and Y142) and a subunit (E721, L724, and N725), give partial resistance to bafilomycin (43, 44). The positions of these residues suggest a binding site for bafilomycin between two adjacent c subunits (pink and magenta) that is accessed via the a subunit (green ribbon). (Scale bars: 25 Å.)

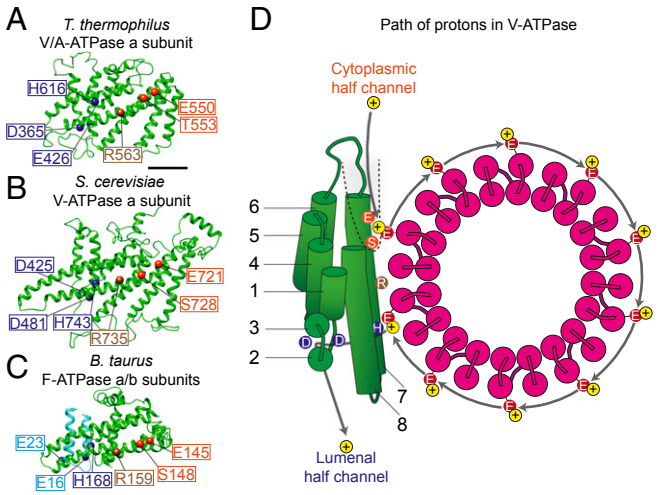

Fig. 5. Model of proton translocation through the a subunit. Models of the a subunit from V/A-ATPase (*A*), V-ATPase (*B*), and F-type ATP synthase (*C*) reveal a similar arrangement of residues important for proton translocation. These similarities suggest the locations of the two offset proton half-channels in the V-ATPase (*D*). A proton (yellow) enters the complex near E721 and S728, which partly form the cytoplasmic half-channel (orange), and neutralizes E137 of a c subunit (red), allowing the c_{10}-ring to turn and enabling another proton to leave the complex via the luminal half-channel, which is composed partly of D425, D481, and H743 (blue). The conserved and essential R735 (brown) resides between these two half-channels. (Scale bar: 25 Å.)

ATP synthase possesses this pair of charged residues (E219 and H245) with positions that indicate that the histidine is on the C-terminal α-helix as in the *T. thermophilus* enzyme. In the *E. coli* enzyme, the mutations E219H and H245E decrease enzyme activity significantly whereas the double mutant E219H/H245E has much less of an effect, suggesting a functional interaction for these residues that is insensitive to which α-helix bears which residue (47). In two α-helices distal to the c-ring, adjacent to the conserved histidine, there are two membrane-embedded acidic residues: D365/E426 in V/A-ATPase and D425/D481 in V-ATPase (Fig. 5 *A* and *B*, blue). In the F-type ATP synthase, the a subunit does not provide a pair of acidic residues, but the b subunit places the conserved residues E16 and E23 in similar positions relative to H168 (Fig. 5*C*, cyan).

We propose that the two offset half-channels in each enzyme involve residues conserved across species and the different types of rotary ATPase. We illustrate this proposed path for protons with the *S. cerevisiae* V-ATPase (Fig. 5*D*). The cytoplasmic half-channel is partly formed by E721 and S728. This half-channel is at least partially accessible from the cytoplasm, as predicted by E721C being identified at the cytoplasmic border. In fact, all residues that have been identified on the cytoplasmic border are clustered around this cytoplasmic half-channel (Fig. 4*A*, pink spheres), suggesting that this region forms an aqueous pore accessible to small labeling molecules such as *N*-ethylmaleimide, but not larger ones like polyethylene glycol maleimide (31). Furthermore, E721 likely participates in bafilomycin binding, suggesting that bafilomycin could inhibit proton transport by blocking the cytoplasmic half-channel. The long and highly charged loop near this half-channel may modulate the function of the cytoplasmic half-channel. The luminal half-channel includes H743 in the C-terminal hairpin, and also D425 and D481 on adjacent α-helices. Residues labeled as luminal that seem to be within the membrane bilayer are clustered around the proposed luminal half-channel (Fig. 4*A*), implying that, like the cytoplasmic half-channel, this aqueous channel may make residues within the channel accessible to small molecules such as *N*-ethylmaleimide. The essential R735, as well as several other residues contributing to V-ATPase activity (including H796, R799, and H801), are placed between the two half-channels. These basic residues would interact favorably with the deprotonated glutamate residue of the c_{10}-ring. In the F-type ATP synthase performing ATP synthesis, this interaction would be required to ensure that protons, driven by the proton motive force, move from the protonating half-channel to the deprotonating half-channel via the hydrophobic environment of the lipid bilayer. In the V-ATPase, or F-type ATP synthase performing ATP hydrolysis, this arrangement of amino acids would ensure that ATP hydrolysis-driven rotation of the c-ring also delivers protons from the protonating to the deprotonating half-channel, but this time with the opposite direction of rotation of the c-ring. This model suggests that, despite their variability in function, conserved patterns of charged membrane-embedded residues control proton translocation in all rotary ATPases.

Methods

Protein Purification. V/A-ATPase was purified from *T. thermophilus* by metal affinity chromatography using an 8× histidine tag at the N terminus of the a subunit (48) as described previously (18), except as noted. Briefly, bacterial membranes were solubilized in buffer (20 mM sodium imidazole, 100 mM sodium chloride, pH 8.0) containing 1% (wt/vol) n-dodecyl β-D-maltoside (DDM) (Anatrace, Inc.) and loaded onto a HisTrap HP column (GE Life Sciences) equilibrated with the same buffer but containing 0.02% DDM. V/A-ATPase was eluted with a linear gradient of imidazole (20–500 mM) in buffer with 0.02% DDM before size exclusion chromatography.

Electron Cryomicroscopy and Image Processing. Purified V/A-ATPase (3.5 μL at 6–8 mg/mL) was applied to nanofabricated holey-carbon film-coated grids with ∼800-nm holes spaced 4 μm apart (49), previously glow-discharged in air for 2 min, and frozen in a liquid ethane/propane mixture in a modified FEI Vitrobot Mark III (50). Samples were imaged with an FEI Tecnai F20 electron microscope operating at 200 kV and equipped with a Gatan K2 Summit direct detector device in counting mode. Then, 2,335 movies were collected with an exposure of five electrons per pixel per second for 15 s and 0.5 s per frame, and a physical pixel size corresponding to 1.45 Å. For tilt pair analysis, the same conditions were used with 7.5 s for both the untilted movie and the movie where the specimen was tilted to 15°. Movie frames were aligned with *alignframes_lmbfgs* (51), and *CTFFIND3* (52) was used to determine contrast transfer function (CTF) parameters from the aligned and averaged frames. Coordinates corresponding to candidate images of individual V/A-ATPases particles were selected from averaged images with *TMaCS* (53). Candidate particle images were extracted from unaligned micrograph movies and corrected for local drift with *alignparts_lmbfgs* (51). A previously measured 2% magnification anisotropy affecting the images and CTF parameters was corrected with *correctmaganisotropy_fspace_list* and *star_fixctfaniso*, respectively (54). Candidate particle images were subjected to 2D and 3D classification in *Relion* (55). Two-dimensional classes displaying distinct features corresponding to intact V/A-ATPase complexes were selected for further analysis. Next, 197,178 and 9,721 particle images were used in *Relion* to build maps of the V/A-ATPase in the first and second conformation, respectively. A density map of the membrane-integral domain of the *S. cerevisiae* V-ATPase a subunit was obtained by segmenting, aligning, and averaging the a subunit from cryo-EM maps of V-ATPase (EMD-6284, -6285, and -6286) and V-ATPase:SidK complexes in *UCSF Chimera* (56). Freehand tests were performed with *Searchrefine_fspace* and *Fastfreehand*, and tilt pair alignment tests were done with *aligntest_histogram* (57), all of which are available at www.sickkids.ca/research/rubinstein.

Map Analysis and Modeling. Local resolution in the cryo-EM maps was estimated with *ResMap* (58) and visualized in *UCSF Chimera*. Homology models were generated with *Phyre2* (59). Crystal structures and homology models were fit into density maps using *MDFF* (60) considering backbone atoms only. For difference maps, the full V/A-ATPase atomic model was converted to a density map with the *molmap* function in *UCSF Chimera*. Evolutionarily covarying residues were identified with *EVcouplings* (24), and the a subunit models were built into the density maps as before (20). Due to the presence of a large, presumably flexible loop in the *S. cerevisiae* V-ATPase a subunit (residues 655–707), for which little density was present in the map, this region of sequence was truncated during modeling (connecting H655 to G709). The loop from residues 651 to 711 was modeled separately with no bias for fitting into density. The second-best-scoring loop of 1,000 output structures was added to the model because the best-scoring loop caused clashes with the c_{10}-ring. This model was subjected to *MDFF* and added back to the a subunit model.

ACKNOWLEDGMENTS. We thank K. Yokoyama for providing the strain of *T. thermophilus* expressing His-tagged V/A-ATPase, S. Lindert for advice on the use of *Rosetta*, and Alexis Rohou, Peter Rosenthal, and Voula Kanelis for a critical reading of this manuscript. This work was supported by Operating Grant MOP 81294 from the Canadian Institutes of Health Research (to J.L.R.). D.G.S. was supported by a Canada Graduate Scholarship from the Natural Sciences and Engineering Research Council (NSERC) and an award from The Hospital for Sick Children. J.Z. was supported by a Doctoral Postgraduate Scholarship from NSERC and a Mary Gertrude l'Anson Scholarship. J.L.R. is supported by the Canada Research Chairs program.

1. Forgac M (2007) Vacuolar ATPases: Rotary proton pumps in physiology and pathophysiology. *Nat Rev Mol Cell Biol* 8(11):917–929.
2. Blair HC, Teitelbaum SL, Ghiselli R, Gluck S (1989) Osteoclastic bone resorption by a polarized vacuolar proton pump. *Science* 245(4920):855–857.
3. Wagner CA, et al. (2004) Renal vacuolar H+-ATPase. *Physiol Rev* 84(4):1263–1314.
4. Frattini A, et al. (2000) Defects in TCIRG1 subunit of the vacuolar proton pump are responsible for a subset of human autosomal recessive osteopetrosis. *Nat Genet* 25(3): 343–346.
5. Karet FE, et al. (1999) Mutations in the gene encoding B1 subunit of H+-ATPase cause renal tubular acidosis with sensorineural deafness. *Nat Genet* 21(1):84–90.
6. Smith AN, et al. (2000) Mutations in ATP6N1B, encoding a new kidney vacuolar proton pump 116-kD subunit, cause recessive distal renal tubular acidosis with preserved hearing. *Nat Genet* 26(1):71–75.
7. Hinton A, et al. (2009) Function of a subunit isoforms of the V-ATPase in pH homeostasis and in vitro invasion of MDA-MB231 human breast cancer cells. *J Biol Chem* 284(24):16400–16408.
8. Zhao J, Benlekbir S, Rubinstein JL (2015) Electron cryomicroscopy observation of rotational states in a eukaryotic V-ATPase. *Nature* 521(7551):241–245.
9. Lau WCY, Rubinstein JL (2012) Subnanometre-resolution structure of the intact Thermus thermophilus H+-driven ATP synthase. *Nature* 481(7380):214–218.
10. Lee LK, Stewart AG, Donohoe M, Bernal RA, Stock D (2010) The structure of the peripheral stalk of Thermus thermophilus H+-ATPase/synthase. *Nat Struct Mol Biol* 17(3):373–378.
11. Oot RA, Huang LS, Berry EA, Wilkens S (2012) Crystal structure of the yeast vacuolar ATPase heterotrimeric EGC(head) peripheral stalk complex. *Structure* 20(11): 1881–1892.
12. Nagamatsu Y, Takeda K, Kuranaga T, Numoto N, Miki K (2013) Origin of asymmetry at the intersubunit interfaces of V1-ATPase from Thermus thermophilus. *J Mol Biol* 425(15):2699–2708.
13. Iwata M, et al. (2004) Crystal structure of a central stalk subunit C and reversible association/dissociation of vacuole-type ATPase. *Proc Natl Acad Sci USA* 101(1):59–64.
14. Murata T, Yamato I, Kakinuma Y, Leslie AG, Walker JE (2005) Structure of the rotor of the V-Type Na+-ATPase from Enterococcus hirae. *Science* 308(5722):654–659.
15. Srinivasan S, Vyas NK, Baker ML, Quiocho FA (2011) Crystal structure of the cytoplasmic N-terminal domain of subunit I, a homolog of subunit a, of V-ATPase. *J Mol Biol* 412(1):14–21.
16. Junge W, Lill H, Engelbrecht S (1997) ATP synthase: An electrochemical transducer with rotatory mechanics. *Trends Biochem Sci* 22(11):420–423.
17. Vik SB, Antonio BJ (1994) A mechanism of proton translocation by F1F0 ATP synthases suggested by double mutants of the a subunit. *J Biol Chem* 269(48):30364–30369.
18. Lau WCY, Rubinstein JL (2010) Structure of intact Thermus thermophilus V-ATPase by cryo-EM reveals organization of the membrane-bound V(O) motor. *Proc Natl Acad Sci USA* 107(4):1367–1372.
19. Allegretti M, et al. (2015) Horizontal membrane-intrinsic α-helices in the stator a-subunit of an F-type ATP synthase. *Nature* 521(7551):237–240.
20. Zhou A, et al. (2015) Structure and conformational states of the bovine mitochondrial ATP synthase by cryo-EM. *eLife* 4:e10180.
21. Morales-Rios E, Montgomery MG, Leslie AGW, Walker JE (2015) Structure of ATP synthase from Paracoccus denitrificans determined by X-ray crystallography at 4.0 Å resolution. *Proc Natl Acad Sci USA* 112(43):13231–13236.
22. Göbel U, Sander C, Schneider R, Valencia A (1994) Correlated mutations and residue contacts in proteins. *Proteins* 18(4):309–317.
23. Cronet P, Sander C, Vriend G (1993) Modeling of transmembrane seven helix bundles. *Protein Eng* 6(1):59–64.
24. Hopf TA, et al. (2012) Three-dimensional structures of membrane proteins from genomic sequencing. *Cell* 149(7):1607–1621.
25. Ovchinnikov S, Kamisetty H, Baker D (2014) Robust and accurate prediction of residue-residue interactions across protein interfaces using evolutionary information. *eLife* 3:e02030.
26. Lau WCY, Rubinstein JL (2012) Subnanometre-resolution structure of the intact Thermus thermophilus H+-driven ATP synthase. *Nature* 481(7380):214–218.
27. Rosenthal PB, Rubinstein JL (2015) Validating maps from single particle electron cryomicroscopy. *Curr Opin Struct Biol* 34:135–144.
28. Bueler SA, Rubinstein JL (2015) Vma9p need not be associated with the yeast V-ATPase for fully-coupled proton pumping activity in vitro. *Biochemistry* 54(3):853–858.
29. Chen R, Runswick MJ, Carroll J, Fearnley IM, Walker JE (2007) Association of two proteolipids of unknown function with ATP synthase from bovine heart mitochondria. *FEBS Lett* 581(17):3145–3148.
30. Carroll J, Altman MC, Fearnley IM, Walker JE (2007) Identification of membrane proteins by tandem mass spectrometry of protein ions. *Proc Natl Acad Sci USA* 104(36):14330–14335.
31. Toei M, Toei S, Forgac M (2011) Definition of membrane topology and identification of residues important for transport in subunit a of the vacuolar ATPase. *J Biol Chem* 286(40):35176–35186.
32. DiMaio F, Tyka MD, Baker ML, Chiu W, Baker D (2009) Refinement of protein structures into low-resolution density maps using rosetta. *J Mol Biol* 392(1):181–190.
33. Rohl CA, Strauss CEM, Misura KMS, Baker D (2004) Protein structure prediction using Rosetta. *Methods Enzymol* 383:66–93.
34. Kawasaki-Nishi S, Nishi T, Forgac M (2001) Arg-735 of the 100-kDa subunit a of the yeast V-ATPase is essential for proton translocation. *Proc Natl Acad Sci USA* 98(22): 12397–12402.
35. Kane PM (1995) Disassembly and reassembly of the yeast vacuolar H(+)-ATPase in vivo. *J Biol Chem* 270(28):17025–17032.
36. Sumner JP, et al. (1995) Regulation of plasma membrane V-ATPase activity by dissociation of peripheral subunits. *J Biol Chem* 270(10):5649–5653.
37. Manolson MF, et al. (1994) STV1 gene encodes functional homologue of 95-kDa yeast vacuolar H(+)-ATPase subunit Vph1p. *J Biol Chem* 269(19):14064–14074.
38. Leng XH, Nishi T, Forgac M (1999) Transmembrane topography of the 100-kDa a subunit (Vph1p) of the yeast vacuolar proton-translocating ATPase. *J Biol Chem* 274(21):14655–14661.
39. Wang Y, Toei M, Forgac M (2008) Analysis of the membrane topology of transmembrane segments in the C-terminal hydrophobic domain of the yeast vacuolar ATPase subunit a (Vph1p) by chemical modification. *J Biol Chem* 283(30):20696–20702.
40. Leng XH, Manolson MF, Liu Q, Forgac M (1996) Site-directed mutagenesis of the 100-kDa subunit (Vph1p) of the yeast vacuolar (H+)-ATPase. *J Biol Chem* 271(37):22487–22493.
41. Leng XH, Manolson MF, Forgac M (1998) Function of the COOH-terminal domain of Vph1p in activity and assembly of the yeast V-ATPase. *J Biol Chem* 273(12):6717–6723.
42. Kawasaki-Nishi S, Nishi T, Forgac M (2003) Interacting helical surfaces of the transmembrane segments of subunits a and c′ of the yeast V-ATPase defined by disulfide-mediated cross-linking. *J Biol Chem* 278(43):41908–41913.
43. Bowman BJ, McCall ME, Baertsch R, Bowman EJ (2006) A model for the proteolipid ring and bafilomycin/concanamycin-binding site in the vacuolar ATPase of Neurospora crassa. *J Biol Chem* 281(42):31885–31893.
44. Wang Y, Inoue T, Forgac M (2005) Subunit a of the yeast V-ATPase participates in binding of bafilomycin. *J Biol Chem* 280(49):40481–40488.
45. Hatch LP, Cox GB, Howitt SM (1995) The essential arginine residue at position 210 in the alpha subunit of the Escherichia coli ATP synthase can be transferred to position 252 with partial retention of activity. *J Biol Chem* 270(49):29407–29412.
46. Meruelo AD, Han SK, Kim S, Bowie JU (2012) Structural differences between thermophilic and mesophilic membrane proteins. *Protein Sci* 21(11):1746–1753.
47. Cain BD, Simoni RD (1988) Interaction between Glu-219 and His-245 within the a subunit of F1F0-ATPase in Escherichia coli. *J Biol Chem* 263(14):6606–6612.
48. Yokoyama K, et al. (2003) Subunit arrangement in V-ATPase from Thermus thermophilus. *J Biol Chem* 278(43):42686–42691.
49. Marr CR, Benlekbir S, Rubinstein JL (2014) Fabrication of carbon films with ~ 500 nm holes for cryo-EM with a direct detector device. *J Struct Biol* 185(1):42–47.
50. Tivol WF, Briegel A, Jensen GJ (2008) An improved cryogen for plunge freezing. *Microsc Microanal* 14(5):375–379.
51. Rubinstein JL, Brubaker MA (2015) Alignment of cryo-EM movies of individual particles by optimization of image translations. *J Struct Biol* 192(2):188–195.
52. Mindell JA, Grigorieff N (2003) Accurate determination of local defocus and specimen tilt in electron microscopy. *J Struct Biol* 142(3):334–347.
53. Zhao J, Brubaker MA, Rubinstein JL (2013) TMaCS: A hybrid template matching and classification system for partially-automated particle selection. *J Struct Biol* 181(3): 234–242.
54. Zhao J, Brubaker MA, Benlekbir S, Rubinstein JL (2015) Description and comparison of algorithms for correcting anisotropic magnification in cryo-EM images. *J Struct Biol* 192(2):209–215.
55. Scheres SHW (2012) RELION: Implementation of a Bayesian approach to cryo-EM structure determination. *J Struct Biol* 180(3):519–530.
56. Goddard TD, Huang CC, Ferrin TE (2007) Visualizing density maps with UCSF Chimera. *J Struct Biol* 157(1):281–287.
57. Baker LA, Watt IN, Runswick MJ, Walker JE, Rubinstein JL (2012) Arrangement of subunits in intact mammalian mitochondrial ATP synthase determined by cryo-EM. *Proc Natl Acad Sci USA* 109(29):11675–11680.
58. Kucukelbir A, Sigworth FJ, Tagare HD (2014) Quantifying the local resolution of cryo-EM density maps. *Nat Methods* 11(1):63–65.
59. Kelley LA, Mezulis S, Yates CM, Wass MN, Sternberg MJ (2015) The Phyre2 web portal for protein modeling, prediction and analysis. *Nat Protoc* 10(6):845–858.
60. Trabuco LG, Villa E, Mitra K, Frank J, Schulten K (2008) Flexible fitting of atomic structures into electron microscopy maps using molecular dynamics. *Structure* 16(5): 673–683.
61. Baker LA, Rubinstein JL (2008) Angle determination for side views in single particle electron microscopy. *J Struct Biol* 162:260–270.
62. Rosenthal PB, Henderson R (2003) Optimal determination of particle orientation, absolute hand, and contrast loss in single-particle electron cryomicroscopy. *J Mol Biol* 333:721–745.
63. Marks DS, et al. (2011) Protein 3D structure computed from evolutionary sequence variation. *PLoS One* 6:e28766.
64. Nugent T, Jones DT (2009) Transmembrane protein topology prediction using support vector machines. *BMC Bioinformatics* 10:159.
65. Sievers F, et al. (2011) Fast, scalable generation of high-quality protein multiple sequence alignments using Clustal Omega. *Mol Syst Biol* 7:539.
66. Eswar N, et al. (2006) Comparative protein structure modeling using Modeller. *Curr Protoc Bioinformatics* Ch 5:Unit 5.6.